Advanced petascale simulations of the scaling up of mixing limited flow processes for materials synthesis

S. Glockner[1], A.M.D. Jost[1], A. Erriguible[1,2]*

[1] Bordeaux INP, University of Bordeaux, CNRS, Arts et Metiers Institute of Technology, INRAE, I2M Bordeaux, F-33600 Talence, France

[2] Bordeaux INP, CNRS, University of Bordeaux, ICMCB, F-33600 Pessac, France

Corresponding author: erriguible@enscbp.fr

Abstract

The paper focuses on the use of petascale simulations to address the open-ended problem of scaling-up continuous flow processes in microfluidics. Some of these processes are mixing limited and so require deep analysis of the scale up effects onto the mixing performance. The scaling up strategy considered is the so-called sizing-up approach based on the conservation of the turbulent dissipation rate in the reactor combined with petascale simulations. High fidelity Direct Numerical Simulations are performed from micro- to milli-scale reactor (up to 11 billion of mesh nodes on 131072 processors) while maintaining the same accuracy of the physical phenomena description (smaller dissipative scales). It leads to confident qualitative estimations of the mixing performance for the different sizing-up scenarios. We show that it is possible to increase up to two orders of magnitude the production rate of the continuous reactor while maintaining an excellent mixing quality, which is very favorable for the material synthesis process.

Introduction

The constant evolution of supercomputer performance over the past 20 years has significantly changed the scientific landscape and the way problems are approached. While algorithms and computational codes have long been ahead of the available computing power, the paradigm has recently been reversed as the available power of petaflop and soon exaflop supercomputers now requires a considerable effort in developing computational codes to take advantage of this power. Nevertheless, this opens up new horizons for better understanding, representing, and predicting physical phenomena as well as for the development of Smart Manufacturing processes, in addition to or even replacing *in situ* experiments. As a demonstration, we propose, for the first time, petascale simulations to answer the open-ended question of scaling up of continuous material synthesis processes. We highlight the value of using the latest supercomputers to study the scaling up without any loss of information, *i.e.* keeping the relevant scale of the physical description to design safe, controlled, and flexible processes. This offers a new path for the industrial development of continuous, sustainable, and scalable technology for the production of innovative materials.

Today, microfluidics is considered one of the most promising technologies for generating innovative materials [1] in a reproducible manner, allowing for efficient mixing, process optimization, and fast screening. This is especially true for materials synthesis for which fast and homogeneous mixing [2] is the key to obtaining a narrow size distribution of particles. However, the problem of moving towards industrialization almost always requires increasing the production and therefore the scale of the reactor. This generally yields to losses in production quality, as the advantages of hydrodynamics at small scales are lost.

The case study, chosen here to demonstrate the proposed approach, is the nanoparticle precipitation in microfluidic reactor by using supercritical carbon dioxide as antisolvent. Recent studies [3] have shown that a combination of the two types of intensification of supercritical fluids and microfluidic reactors (μSAS) can significantly improve the performance and reproducibility of antisolvent processes. Moreover, it has recently been proven that turbulent conditions can be achieved in high pressure microfluidic devices [4], resulting in ultra-fast mixing times as small as 10^{-4}-10^{-5}s which are highly favorable for the synthesizing of organic nanoparticles. However, it should be noted that the mass flow rates used in the microreactors are much lower than those used for large reactors. As a result, even though the former offer excellent mixing performances and better control of the conditions the latter have the big advantage of larger production rates. Finally, continuous flow processes [5] currently offer greater advantages compared to batch processes as the former can maintain constant flow operating conditions and achieve very efficient mixing. However, one of the main drawbacks of the microfluidic flow processes remains its limited adaptation to an industrial scale [6,7]. It is commonly accepted that numbering up [8–10] is probably the best approach, compared to sizing up [11,12], to maintain an excellent control of the operating conditions and efficient mixing. However, scaling up through numbering up requires thousands of reactors to achieve significant production thereby posing the challenging task of a uniform fluid distribution [5,10,13].

One of the solutions could be to seek a compromise between sizing up and numbering up [14]. A first step of sizing up could be a decrease in the number of units of the system to guarantee a uniform distribution of the fluids in the system. As such, the first question that needs to be answered is: can a continuous micro-scale/milli-scale reactor operate at the same flow rates as a large scale reactor while maintaining an excellent mixing performance? To answer this question, it is imperative to propose an efficient strategy to determine the relevant size of the

flow reactor that can strike a good balance between size and production ability. The classical approach, consisting in using the canonical similitude law, tends to fail in giving appropriate solutions for the continuous processes. This is inherent to the complexity of the dynamic system as many parameters interact in the continuous flow processes. Therefore, even if satisfactory results with partial or complete similarity methods can be found in literature [15,16], a simulation-based strategy appears to be a suitable solution to find a good candidate for the continuous processes. For this purpose, direct numerical simulations (DNS) - which do not include any extra modeling of turbulence since the finest dissipative scale are solved - are the most accurate way to capture the interactions between turbulence and species mixing. Although DNS has been mainly first restricted to canonical cases, the continuous development of supercomputers has expanded its applicability to the design of complex systems. DNS yields information on the flow and mixing characteristics unattainable through in situ experiments.

In this paper, it will be shown that high performance computing (HPC), through petascale numerical simulations, is a relevant and promising tool to study and analyze scale up scenarios for chemical engineering processes and to further demonstrate that continuous flow processes are competitive. The current case study is the supercritical microfluidic antisolvent process for which we propose - for the first time - high fidelity DNS simulations for micro-scale to milli-scale resulting in an increase of up to 90 times the initial production flow rate. The scaling up strategy takes advantage of HPC and latest supercomputers to pursue simulations of larger reactors while maintaining the same accuracy of the physical phenomena description simulated in the micro reactors (smaller dissipative scales). As such, special care must be taken to establish the strategy used to determine the larger flow rates and reactor dimensions as well as the numerical strategy needed to run petascale simulations. Results confirm both the fact that it is possible to increase the size of the reactor whist maintaining excellent mixing conditions.

Materials and Methods

Scaling up strategy. As previously introduced, we have chosen to consider the supercritical antisolvent microfluidic process for which the mixing performance is the key point yet to be demonstrated [3]. Therefore, in this article we focus on the DNS simulations of the hydrodynamic and mixing phenomena. The process consists of a simple tube-in-tube reactor as shown in figure 1. The solution, solvent, is injected in the inner tube, diameter Di, whereas the supercritical CO2, acting as antisolvent, is injected in the coflow between the diameters Do and Dext. The typical pressure and temperature of p = 100 bar and T = 40°C, respectively, are chosen and the reference case is that at microscale. The mean Reynolds number $Re = \frac{D_{ext}\bar{\rho}\,\bar{u}}{\bar{\mu}}$ is calculated inside the outer tube by considering the mean values of velocity $\bar{u}$ [17], viscosity $\bar{\mu}$, and density $\bar{\rho}$. The mean properties are estimated according to the molar ratio of 91% between the solvent and the antisolvent. It should be noted that an important constraint of the current process is the pressure loss. Actual back pressure regulator technology is able to absorb pressure losses of a few tens of bar. The classical approach used to compute the pressure loss ΔP in the inner tube, outer tube, and coflow zone is $\Delta P = \frac{f}{D}\frac{\rho u^2}{2}$ with $f = 0.3164Re^{-0.25}$ being the Blasius friction factor for turbulent flow in pipes, u the velocity, and D the diameter in the considered zone (coflow zone D = D_{ext}-D_o, inner tube D = D_i, outer tube D = D_{ext}).

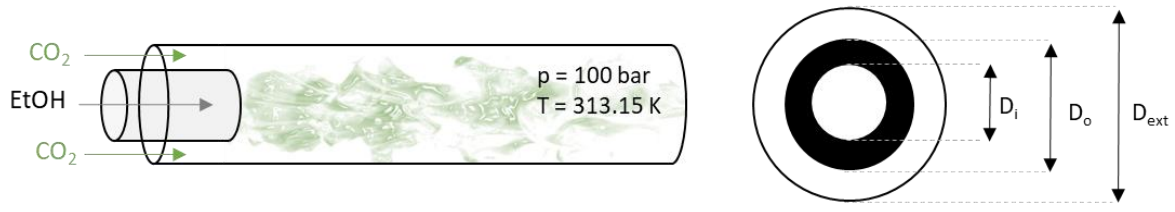

Fig 1. Diagram of the tube-in- tube reactor. The solution, solvent, is injected in the inner tube, diameter D_i, whereas the supercritical CO_2, acting as antisolvent, is injected in the coflow between the diameters D_o and D_{ext}. The typical pressure, temperature and solvent/antisolvent molar ratio are 100 bar, 40°C and 91%, respectively, are chosen.

It has been widely reported that the mixing is governed by the dissipation rate of the turbulent kinetic energy [18]. Thanks to the Kolmogorov theory, Baldyga and Bourne [19] have established a direct relation between the dissipation rate and the mixing time. From a mixing point of view, the most important global parameter is the dissipation rate of the turbulent kinetic energy ε and, in the tube, it can be approximated through dimensional analysis as $\varepsilon \approx \frac{f}{2}\frac{\overline{u^3}}{D_{ext}}$ with *f* being the Blasius friction factor. It should be pointed out that as the key point of the process is to obtain an excellent mixing performance, the scaling up strategy consists in conserving the global turbulent kinetic energy dissipation rate ε in the reactor by adjusting the inlet mass flow rates and dimensions of the tube. In literature this strategy is coined as "constant energy dissipation scale up*"* [20] or "constant pressure drop approach" [13]. Henceforth, the global turbulent kinetic energy dissipation rate is referred to as the global dissipation rate.

The initial case is chosen at microscale with D_i =100 μm and D_{ext} = 250 μm (Fig. 1). The initial mass flow rates of the solvent (inner tube) and CO_2 (coflow zone) are 400 μl/min and 3000 μl/min, respectively, leading to a solvent-antisolvent ratio of 91% mol. The global dissipation rate ε is estimated at 235 W/kg leading to a Kolmogorov scale of about a micrometer. As the Schmidt number is about 2.6 the Batchelor scale $\lambda_B = \frac{\lambda_K}{\sqrt{Sc}}$ it is approximately in the same range as the Kolmogorov length scale. Therefore, to capture all the mixing scales and to yield accurate results the mesh size of the simulation is chosen to be on the order of the micrometer (see Table 2). As previously mentioned, to determine the optimal flow rates of the reactor needed to maintain a good mixing, we chose to consider the constant energy dissipation scale up method. We, therefore, imposed the different sizes of the reactor (see dimensions cases 1, 2, 3, 4 in table 1) and through a minimization algorithm the flow rates of the solvent and antisolvent (Q_{EtOH} and Q_{CO2} in table 1) are optimized. The target of this optimization problem is the global dissipation rate ε (table 1) which coincides to the one determined for the initial

case 0. The problem is closed by adding two constraints: 1) the pressure drop in the annular/coflow zone must be less than 50 bar and 2) the ratio of the molar flow rate of solvent and antisolvent must be 91%, as for initial case 0. This strategy yields 5 cases bringing the production flow rate up to nearly 90 times the initial production flow rate. The main operating conditions of the simulation cases are presented in Table 1.

Case	R	QEtoh ($\mu l/min$)	Qco2 ($\mu l/min$)	VEtoh (m/s)	Vco2 (m/s)	$\bar{u}$ (m/s)	CO2% mol	ε (W/kg)	Re	Max. Δp (bar/m)	Di (μm)	Do (μm)	Dext (μm)
0	1	400	3000	0.87	3.35	1.47	91	235	5245	16	100	170	250
1	9	3539	25542	1.23	6.08	2.18	91	235	18496	21	250	450	600
2	31	12400	89495	1.07	9.32	2.75	91	235	38884	31	500	800	1000
3	55	21867	157820	1.89	6.25	2.75	91	235	54420	5	500	800	1260
4	87	34655	250117	3.00	5.61	3.33	91	235	71494	3	500	800	1520

Table 1. Operating conditions of the simulation cases. R: production ratio. QEtoh: volume flow rate of solvent. Qco_2: volume flow rate of antisolvent. VEtoh: velocity in inner tube. Vco_2: velocity in the coflow zone. Max. ΔP: the maximum calculated linear pressure drop in the reactor (injector or coflow zone).

Governing equations of the fluid mixing. All the equations established in previous studies [4,17,21], are briefly presented. The hydrodynamic Navier-Stokes equations are solved for totally miscible and isothermal fluids. It is generally considered that a supercritical fluid is compressible (especially when close to the critical point). In our case, the fluid is quite above the critical point so the isothermal compressibility is relatively low (between 10^{-8} and 10^{-9} Pa^{-1}). Furthermore, as the flow is isothermal the thermo-compressible effects are negligible. The comparison of simulations between an incompressible formulation with variable density and a full compressible formulation [22,23] has shown that the results were very close. As the CPU time was optimized within the incompressible formulation, as described in the numerical methodology section, we considered this formulation to solve the hydrodynamics phenomena.

As such, the fluid mixture flow composed of fully miscible ethanol solvent and CO_2 antisolvent, is governed by the Navier-Stokes equations:

$$\boldsymbol{\nabla}.\mathbf{u} = \mathbf{0} \quad (1)$$

$$\rho\left(\frac{\partial \mathbf{u}}{\partial t} + \mathbf{u}.\nabla\mathbf{u}\right) = -\nabla p + \nabla.\left(\mu(\nabla\mathbf{u} + \nabla^{\mathrm{T}}\mathbf{u})\right) \quad (2)$$

where **u** is the fluid velocity. *p* is the pressure, ρ is the fluid density, and μ is the fluid viscosity. As the Froude number is much higher than one resulting from a high Reynolds number flow for all reactor sizes in the range from micro- to milli-, gravity is neglected in the model.

The Reynolds number of the simulation ranges from 5245 to 71494. One of the strengths of the current work is its ability to perform DNS up to the Kolmogorov scale, thereby not requiring any turbulence model and yielding more accurate results.

At the inflow boundary, a laminar Poiseuille flow profile is imposed for the injector whereas the streamwise velocity component *ux* has a constant profile in the coflow and is superimposed by a uniformly distributed fluctuations ranging between ±0.05 *ux* [21]. A zero-gradient boundary condition is applied at the outlet boundary (length of the pipe is long enough to justify this approximation) and no-slip boundary conditions at the remaining boundary conditions.

The species mass fraction of the ethanol solvent is governed by the following advection/diffusion equation

$$\rho\frac{\partial x_{EtOH}}{\partial t} + \nabla\cdot(\rho x_{EtOH}\boldsymbol{u} + \rho D_{EtOH}\nabla x_{EtOH}) = 0 \quad (3)$$

where D_{EtOH} is the diffusion coefficient.

The species mass fraction of the antisolvent CO_2 is given by

$$x_{CO_2} = 1 - x_{EtOH} \quad (4)$$

The thermophysical properties of the CO_2 and ethanol fluid mixture are computed thanks to the cubic Peng-Robinson equation of state coupled with the Van der Waals mixing rules [24]:

$$p = \frac{RT}{V_m - b_m} - \frac{a_m}{V_m(V_m + b_m) + b_m(V_m + b_m)} \quad (5)$$

where V_m is the molar volume ($V_m = Z_m RT/p$ with Z_m the compressibility factor) and a_m and b_m are the attraction parameter and the co-volume parameter of the mixture, respectively:

$$a_m = \sum_{i=1}^{n} \sum_{j=1}^{n} x_i x_j a_{ij} \quad \text{and} \quad b_m = \sum_{i=1}^{n} \sum_{j=1}^{n} x_i x_j b_{ij} \quad (6)$$

with

$$a_{ij} = (1 - k_{ij})(a_{ii} a_{jj})^{0.5} \quad b_{ij} = (1 - l_{ij}) \frac{b_{ii} + b_{jj}}{2} \quad (7)$$

and

$$a = \frac{0.45724 \alpha R^2 T_c^2}{p_c} \quad b = \frac{0.0778 R T_c}{p_c} \quad (8)$$

$$\alpha = \left(1 + (0.37464 + 1.5422\omega - 0.26992\omega^2)\left(1 - \sqrt{\frac{T}{T_c}}\right)\right)^2 \quad (9)$$

where the binary interaction parameters k_{ij} and l_{ij} are given by

$$k_{ij} = -0.4652 e^{-3} T + 0.238 \quad (10)$$

$$l_{ij} = -0.8116 e^{-3} T + 0.2491 \quad (11)$$

The viscosities of the pure fluids CO_2 and ethanol are obtained from the NIST database and the viscosity of the fluid mixture is given by

$$ln\mu_m = x_{EtOH} ln\mu_{EtOH} + x_{CO_2} ln\mu_{CO_2} \quad (12)$$

Finally. the diffusion coefficient of ethanol in CO_2 is given by Hayduck-Minhas correlation [17]:

$$D_m = 1.33e^{-7}T^{1.47}V_{EtOH}^{-0.71}\mu_{CO_2}^{\frac{10.2}{V_{EtOH}-0.791}} \quad (13)$$

where V_{EtOH} is the molar volume of pure ethanol computed by the Peng-Robinson equation of state.

Numerical modeling and computational strategy. To tackle the numerical challenge of DNS of a supercritical microfluidic antisolvent process in large tubes, the Cartesian grid-based finite volume CFD open-source code Notus [25] (developed in-house) is used. The code is based on the finite volume method on a Cartesian grid with explicit or implicit discretization of the governing equations. The velocity-pressure coupling is solved thanks to the Goda pressure correction method (time splitting) [26]. Notus has been widely verified and validated for single and multiphase flows (see for instance [21,25,27,28]). Concerning the present case, similar simulations have been validated by micro-PIV [17] and experimental validation for simulations including nucleation and growth phenomena have also been performed [3,29].

For the current study, the code has been adapted to modern petascale supercomputers such as the Joliot-Curie supercomputer. It is based on AMD Epyc2 dual processor nodes with each processor having 64 cores, resulting in a total of 293 376 cores. This opens new possibilities in numerical simulations. The upscaling of Notus from thousands of cores to more than a hundred thousand cores has been made possible thanks to fully explicit numerical schemes that considerably reduce the amount of time spent in the linear system solvers. This approach takes advantage of favorable physical fluid characteristics that do not significantly reduce the Courant–Friedrichs–Lewy condition and thus maintain a low total number of time iterations of

the simulations. A second order total variation diminishing (TVD) centrally discretized scheme with flux-limiters is used, which ensures a good compromise between accuracy and CPU time. This approach has been recently proven to be efficient for DNS of supercritical microfluidic antisolvent process in micro-tube [21]. The only linear system that needs to be solved is associated with the pressure variable for which the very efficient PFMG geometric multigrid solver of the Hypre library [30] is used. Moreover, for such a large number of cores some communication bottlenecks between MPI processes appear, and have been overcome thanks to a change in the parallel programming paradigm, from a full MPI to a hybrid OpenMP/MPI approach. Before running large scale simulations, an analysis of the performance of the Notus code on such an architecture and programming environment is performed. Table 2 shows that the average number of cells per processor is reduced to 40^3 while keeping a very good scalability, thereby allowing to perform simulations on 131072 cores for the largest case we propose. This point is crucial to attain reasonable total run times of around only 48 hours for a mesh size of more than 10 billion cells.

Care must also be taken with the file system Input/Ouput (I/O) and data visualization strategies. Two kinds of I/O are pursued. The first one deals with the code's checkpoint/restart procedure which needs to write on the parallel file system all the necessary information to restart a simulation without any loss of information. This leads to huge files of up to 3.6 TB which, thanks to the ADIOS library [31], are efficiently written. On a Lustre parallel file system, aggregate I/O rates of around 50 GB/s have been measured. Moreover, for visualization purposes, I/O performance constraint as well as a data file format that support domain decomposition while reading a file with a parallel visualization software (VisIt for this study) must be satisfied. For this purpose. the HDF5 Pixie file format is chosen and yields I/O performances of around 10 GB/s. The total amount of data needed to realize the proposed video of the present article is around 100 TB.

		1 thread / process MPI		2 threads / process MPI		4 threads / process MPI		8 threads / process MPI	
Nb of Cores	**Mesh size**	Notus (s)	Hypre (s)	Notus (s)	Hypre (s)	Notus (s)	Hypre (s)	Notus (s)	Hypre (s)
128	8.2E+06	6.1	3.6	5.6	3.3	6.1	3.4	7.8	3.5
512	3.3E+07	6.1	4.0	6.1	5.8	6.5	4.5	7.9	4.3
2048	1.3E+08	6.6	4.7	6.4	4.3	6.6	4.2	8.5	5.9
8192	5.2E+08	7.2	5.6	6.9	5.1	7.3	5.1	9.1	5.5
32768	2.1E+09	8.7	9.1	8.4	7.1	8.5	6.6	9.9	7.2
131072	8.4E+09	41.6	34.1	14.5	13.0	**14.1**	**10.5**	19.1	11.7

Table 2. Weak scalability study with 40^3 cells per core for an OpenMP/MPI strategy. The full MPI approach results in communication bottlenecks for more than 32768 cores; the 4 OpenMP threads / process MPI approach reduces the CPU time of the Notus code and of the Hypre library by a factor 3.

Results

The main operating conditions of the simulation cases are presented in Table 1. To capture all the mixing scales and to yield accurate results the mesh size of the simulation is chosen to be on the order of the micrometer (see Table 3). As further demonstrated, the Kolmogorov and Batchelor scales are on the same order of magnitude which is particularly advantageous for the current numerical simulations. Indeed, by solving the flow characteristics at the Kolmogorov length scale we resolve all of the mixing scales. The simulations were performed on 512 to 131072 processor cores on the Joliot Curie supercomputer, ranked 38th on the Top 500 list of the largest supercomputers [32] with mesh sizes ranging from 55 million to 11 billion (see Table 3). This yields extremely accurate results especially in terms of the mixing performance of the reactors.

Case	*Reactor Length (mm)*	*Rector diameter(mm)*	*Mesh size*	*Approx. Number of cells ($x10^9$)*	*Mesh step size ($x10^{-6}$)*	*Number of processors*
0	3	0.2	2000 x 167 x 167	0.055	1.5	512
1	4	0.6	4000 x 600 x 600	1.4	1	32768
2	5	1	5000 x 1000 x 1000	5	1	32768
3	5	1.26	5000 x 1260 x 1260	8	1	65536
4	5	1.52	5000 x 1520 x 1520	11.5	1	131072

Table 3. Reactor dimensions, mesh size and number of processors used for cases 0 to 4.

Verification of resolved finest scales. First, to verify that the energy dissipation scales, *i.e.* the Kolmogorov length scales, are resolved in all the simulations currently pursued, analysis of the 1D turbulence spectra E_u and E_x of the root mean squared (RMS) of velocity and of the mass fraction fluctuations. Respectively, expressed as $\langle u_x' u_x' \rangle = \int_0^\infty E_u(k)dk$ and $\langle x_s' x_s' \rangle = \int_0^\infty E_x(k)dk$. Respectively, are performed. In the former relations, *k* is the wave number, and u_x' and x_s' are the velocity and mass fraction fluctuations, respectively. The fluctuation of a variable is defined as the difference between the variable's instantaneous value and its time averaged. i.e. $u_x = \bar{u} + u_x'$, where $\bar{u}$ is the time averaged value. The turbulence spectra are then obtained by performing a Fast Fourier Transform with a Hann window of the desired quantities along the centerline of the domain and are shown in Fig. 2. As expected, regardless of the case, the spectra decay with slopes of approximately -5/3, as predicted by the Kolmogorov theory. It is widely accepted in the turbulence community that a slope of -5/3 is a good indicator that a simulation has captured the smallest scales of the turbulence. Moreover, as already mentioned above, as the Batchelor scales are on the same order of magnitude as the Kolmogorov scales, all the scales of interest of the mixtures have been captured which is the *sine qua non* condition of the forthcoming quantitative analysis of the mixture A precise analysis and interpretation of the second part of the mass fraction turbulence spectra is still an open question. As detailed in a comprehensive review [33], a slope of -1 is only valid for Sc>>1.

For Sc = O(1), such as in our case, it is shown that the slope is not determined (probably around -3, a value close to the one obtained in the present work).

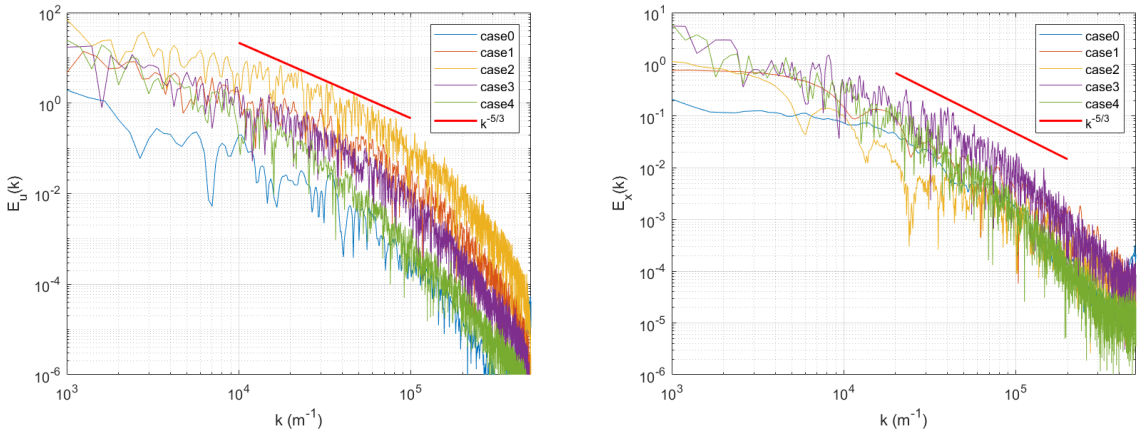

Fig. 2. Turbulence spectra analysis. 1D turbulence spectra for velocity RMS (right) and mass fraction fluctuation (left). The turbulence spectra are then obtained by performing a Fast Fourier Transform with a Hann window of the desired quantities along the centerline of the domain and are shown in Fig. 2. As expected. regardless of the case. the spectra decay with slopes of approximately -5/3, as predicted by the Kolmogorov theory.

Qualitative flow and mixing analysis. As the current study is focused on the evaluation of the mixing performance of the tube-in-tube processes, only the analysis of concentration fields of the species is presented. Fig. 3 shows the evolutions of the ethanol mass fraction in the median planes of the reactors for each configuration. As a first observation, the mixing of the species is correctly achieved in the domains and seem to be very fast. It should be recalled that the constraints imposed when determining the conditions for the scaling, such as the ratio of flow rates and the overall dissipation rate in the system, lead to different inlet velocity ratios which, subsequently, result in different jet shapes. However, overall, there are two different configurations. The first one, visible in cases 0, 3, and 4 is characterized by a relatively long jet. It should be noted that the potential core zone may vary significantly (especially in case 3) for this first configuration. This jet morphology appears in the case of moderate velocity ratios (3 and 4). The second configuration concerns high velocity ratios such as those used in cases 1

and 2. In this configuration, the internal solvent jet breaks up as soon as it leaves the injector. This is due to a very high velocity in the coflow (up to 9 m/s in case 2) resulting in extremely intense and fast mixing.

As discussed in our previous paper [21], the turbulent transition of these coaxial jets is due to the significant development of primary and secondary Kelvin Helmoltz instabilities resulting from strong shear stress between layers of different densities. DNS emphasizes the multitude of scales and highlights the primary and secondary KH instabilities. These are clearly visible. for example, in case 4 in Fig. 3 and 4. Even though a simple visual analysis of the mass fraction fields leads to the conclusion that the mixtures are very good, the performances of the mixtures are further analyzed in order to quantify the influence of the changes of scale and its relevance in terms of processes.

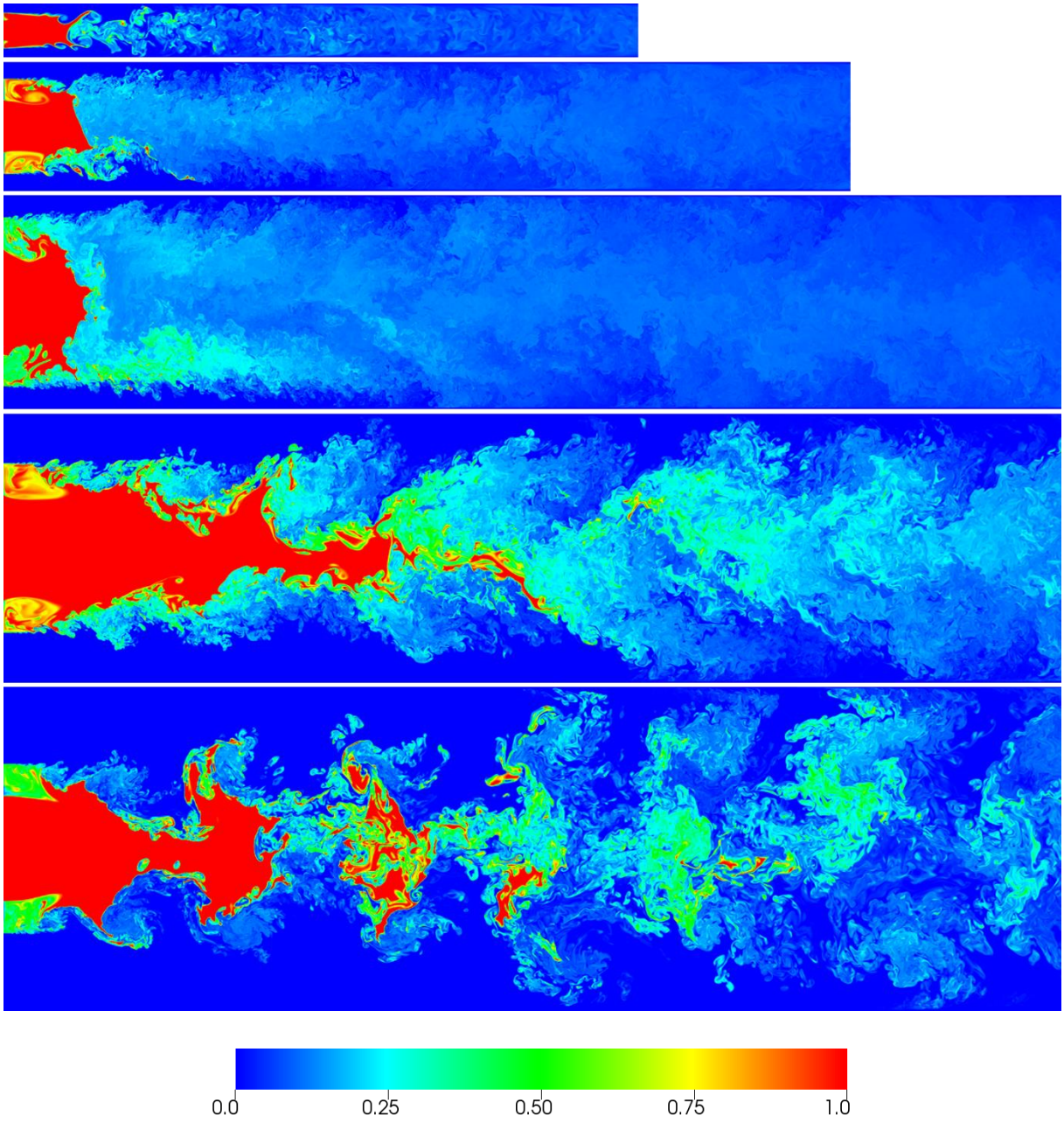

Fig. 3. Instantaneous mass fraction fields in the median planes of the reactors for the cases 0 to 4 (top to bottom). As a first observation. the mixing of the species is correctly achieved in the domains and seem to be very fast. Secondly. different jet shapes are observed. Cases 0, 3, and 4 are characterized by a relatively long jet. With high velocity ratios such as those used in cases 1 and 2 the internal solvent jet breaks up as soon as it leaves the injector. This is due to a very high velocity in the coflow (up to 9 m/s in case 2) resulting in extremely intense and fast mixing. Full length domains are presented, true scales between the cases are also respected.

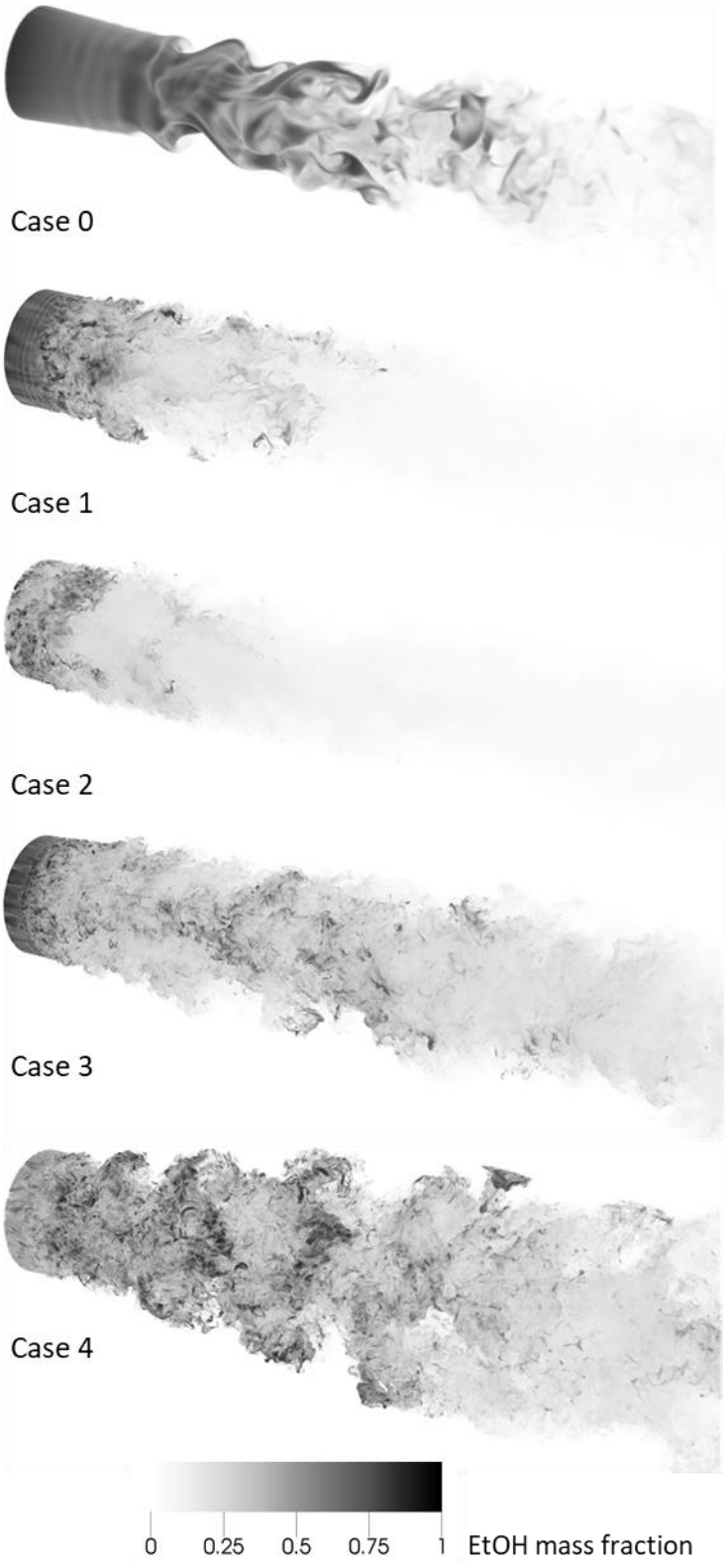

Fig 4. Instantaneous concentration volume renderings for the cases 0 to 4 (top to bottom) - see additional videos 2-6. The turbulent transitions of the coaxial jets is due to the significant development of primary and secondary Kelvin Helmoltz instabilities resulting from strong shear stress between layers of different densities. DNS emphasizes the multitude of scales and highlights the

primary and secondary KH instabilities. Scale is different for each case to better emphasize the description of the instabilities (domains are truncated).

Quantitative mixing analysis.

To estimate the performance of the mixing in the different cases, we have chosen to analyze mixing both from a global point of view and from a local point of view thanks to the intensity of segregation and to the local estimation of micromixing time, respectively.

Global evolution of the mixing performance are checked through the segregation intensity of mixing [4,17,21] based on the length of the reactor. The intensity of segregation is defined by [34]:

$$\boldsymbol{I_m} = \frac{\sum_1^N (x_{EtOH} - \overline{x_{EtOH}})^2}{N(\overline{x_{EtOH}}(x_{EtOH} - \overline{x_{EtOH}}))} \quad (14)$$

A segregation value of 1 and 0 correspond to total segregation between the species and perfect mixing, respectively. This index is calculated for each abscissa x in the yz plane [17]. Figure 5 we propose the evolution of the segregation index as a function of the length for each reactor.

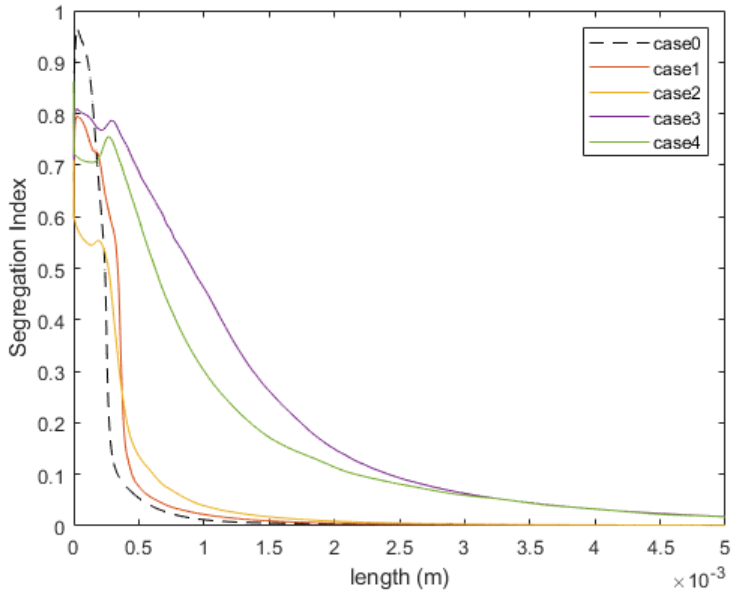

Fig. 5. Evolution of the segregation intensities for all cases in function of the length of the reactor

Although mixing is achieved in a very short distance regardless of the case considered, two different situations can be clearly distinguished. The first concerns cases 1 and 2 for which the mixing seems to be extremely rapid and complete and occurs in the same range than the initial case (case 0). The second one concerns the bigger reactors which follows the same trend, a very good mixing, but with a slight decrease of the mixing performance compared to the original one. Indeed, the intensity of segregation decreases at a slower rate and does not reach zero at the end of the reactor. The intensity is equal to 0.018 at the end of the reactor indicating a good, but not fully complete, mixing. This remark is consistent with the evolution of the mass fraction field (figure 3) for the two larger reactors for which some concentration gradients are still present at the outlet. It should be noted, however, that the increases in the dimensions of the reactor are accompanied by increases in the external diameters to maintain acceptable pressure drops in the system. Therefore, the confinement of the jets becomes less important and tends to decrease the mixing performance of the reactors.

To complete the mixing performance analysis we currently propose an estimation of the mixing time. For that, we analyzed the statistic distribution of the local mixing time. As demonstrated in literature [18], mixing can occur at different scales, such as macro-, meso- and micro-scale. Many studies have emphasized the direct influence of the micromixing in obtaining favorable conditions for the process. Baldyga and Bourne [19] first proposed a definition of the micromixing time. They deduced from Kolomogorov's theory that this crucial characteristic time is directly correlated to the kinematic viscosity and the turbulent kinetic energy dissipation rate:

$$t_m = 17.24\sqrt{\frac{\upsilon}{\varepsilon}} \tag{15}$$

In this equation, the value of the constant (17.24) is subject of discussion in literature. Recently [35], authors have suggested a value of 12.7, very close to the constant of the hydrodynamic

lifetime of vortex [19]. As this difference does not affect the mixing analysis of the present study, we considered in the present work the original model from Baldyga.

Direct numerical simulations allow the accurate determination of the local evolution of the dissipation rate of the turbulent kinetic energy ε. The latter is defined by:

$$\varepsilon = 2\nu \left[\begin{array}{c} \left(\frac{\partial u_x'}{\partial x}\right)^2 + \left(\frac{\partial v_y'}{\partial x}\right)^2 + \left(\frac{\partial w_z'}{\partial x}\right)^2 + \left(\frac{\partial u_x'}{\partial y}\right)^2 + 2\left(\frac{\partial v_y'}{\partial y}\right)^2 + \left(\frac{\partial w_z'}{\partial y}\right)^2 \\ + \left(\frac{\partial u_x'}{\partial z}\right)^2 + \left(\frac{\partial v_y'}{\partial z}\right)^2 + 2\left(\frac{\partial w_z'}{\partial z}\right)^2 + 2\left(\frac{\partial u_x'}{\partial y}\frac{\partial v_y'}{\partial x}\right) \\ +2\left(\frac{\partial u_x'}{\partial z}\frac{\partial w_z'}{\partial x}\right) + 2\left(\frac{\partial w_z'}{\partial y}\frac{\partial v_y'}{\partial z}\right) \end{array} \right] \quad (16)$$

with u_x', v_y', w_z' the velocity fluctuations in each direction.

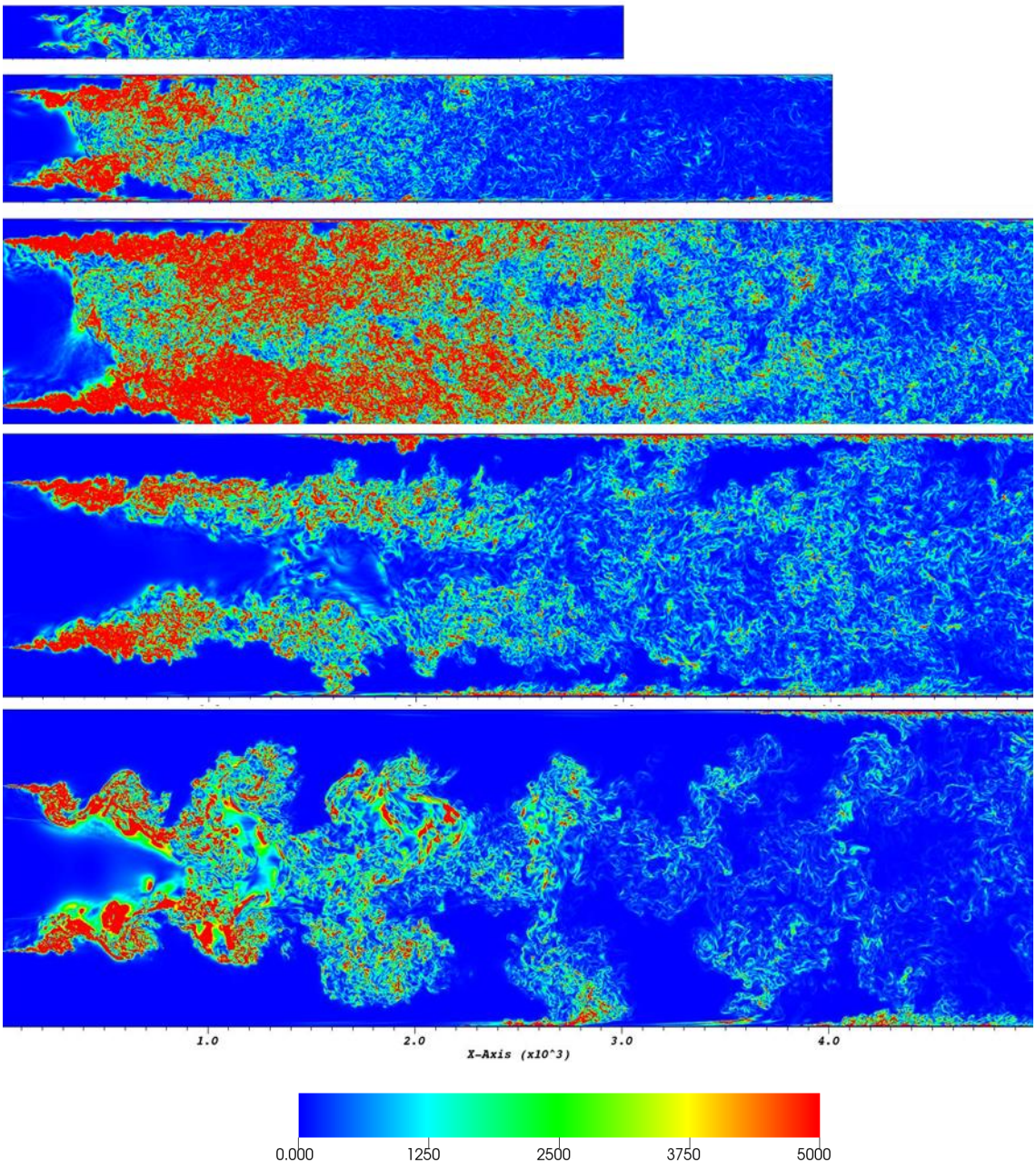

Figure 6: Instantaneous turbulent kinetic energy dissipation rate for the cases 0-4.

Figure 6 shows the fields of the dissipation rate of the turbulent kinetic energy calculated by equation 16 in the median plane of the reactors for each case and allows one to locate the areas of intense mixing and therefore provide information on the mixing. The range of the TKE dissipation rate is similar for all simulations indicating that mixing occurs probably in the same temporal range. As already observed in figure 5, mixing occurs in a short length after the tip of

the injector. It can be observed that for case 1 and 2, strong mixing zones are observed in the periphery of the jet due to a high velocity ratio between the injection and coflow zones. To estimate the characteristic mixing time in the reactor, TKE dissipation rate fields (Fig.6) have been used to estimate the micromixing time according to the equation (15). As such, to compare the mixing performances of the reactors, the micromixing time of each cell in the domains is directly deduced from the dissipation rate of the turbulent kinetic energy (Fig.6). Figure 7 only shows the normalized volume distributions of the micromixing time in the median planes of each reactor. Due to the reactors' cylindrical geometry, the distribution in the median plan is statistically representative of the 3D configuration. The first important result is the mean value of the micromixing time obtained for the initial case (case 0). As expected, we found a mean value between 100 and 200 μs, indicating a very fast mixing leading to very favorable conditions for material synthesis. The previous observation of the mass fraction fields of cases 1 and 2 suggests an extremely fast mixing and is confirmed by the narrow distributions of the micromixing time for which the average values are around 50 μs. The high velocity ratios and the important confinement in the reactors seem to lead to very favorable mixing efficiency conditions. Cases 3 and 4 result in mean micromixing times that are slightly higher than the initial case at around 200 μs. These are still excellent mean mixing times for the elaboration of materials.

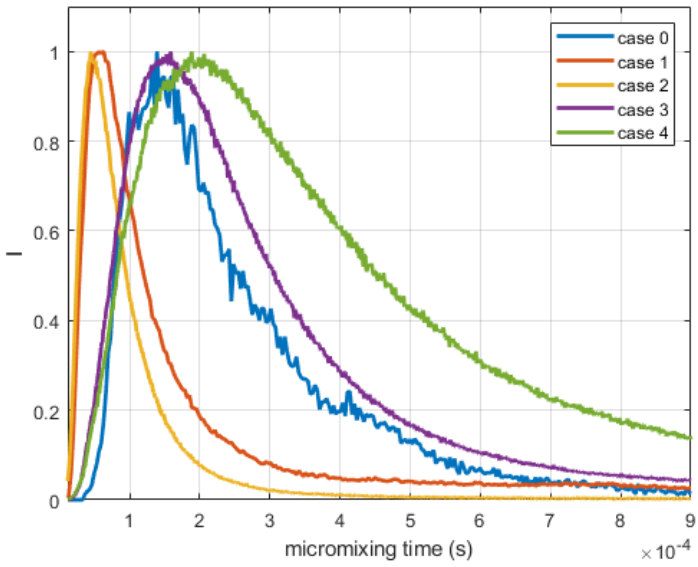

Fig. 7. Normalized volume distributions of the micromixing time in the median planes of the reactors for all cases. For case 0 we found a mean value between 100 and 200 µs. indicating a very fast mixing. Cases 1 and 2 suggests an extremely fast mixing and is confirmed by the narrow distributions of the micromixing time for which the average values are around 50 µs. Cases 3 and 4 result in mean micromixing times that are slightly higher than the initial case at around 200 µs. These are still excellent mean mixing times for the elaboration of materials.

It is also interesting to note that the distributions of the mixing time for cases 3 and 4 are significantly wider than the previous ones. This is probably due to the lower velocity ratios and reduced confinement. These observations support the conclusion given by the evolution of the intensity of segregation in the reactor. So, even if there are some differences in the distributions of the mixing time, the order of magnitude is well preserved and shows that the currently proposed strategy allows significant increases in the production flow rate while keeping very favorable mixing conditions. It is worth noting that the increases in the dimensions of the reactor are accompanied, in our simulations, by a slight but acceptable decrease of the mixing performance. This suggests that the scaling up strategy can only be pursued up to a certain dimension, after which it will be impossible to combine increased production and conservation of mixing performance. Let us note that in our study, the last case corresponds to the maximum

flow rate achievable by the usual CO_2 pump. Finally, increases of the Reynolds numbers due to the increase in reactor size is needed to maintain the mixing performance. Furthermore, the velocity ratio is also very important and a high value contributes to increases in the mixing performance as demonstrated for the cases 1 and 2.

Conclusion

In this paper we are interested in the open-ended problem of the scaling up of a continuous flow process. Towards this end, we propose direct numerical simulations from lab/academic scale to production/industrial scale. The strategy consists in increasing the dimensions of the reactor whilst maintaining the same accuracy of the physical phenomena description. This results in DNS from micro-scale reactors to milli-scale reactors with production rates of up to two orders of magnitude larger. From a chemical engineering point of view, these simulations show that it is possible to increase the volume of the continuous reactor (the diameter has been enlarged by a factor of 6) while maintaining an excellent mixing quality, which is very favorable for the material synthesis process. With a larger reactor, the production rate has increased by a factor 100 while conserving the excellent performance of mixing, thereby indicating that this first step of sizing up yields a decrease, by two orders of magnitude, in the number of units in the numbered-up platforms. This leads to an assurance of a better distribution of the fluid in the system and also a reduction in the manufacturing costs and complexities.

To the best of our knowledge, the simulation performed on a mesh size of 11 billion cells and 131072 processors is the largest realized in the field of continuous flow processes. It shows that petascale high fidelity numerical simulations is an emerging and efficient tool for the analysis of different scaling up scenarios or reactor designs in the field of chemical engineering that open new insights at industrial scale. Indeed, all relevant space and time scales are resolved which gives information on the flow and mixing characteristics unattainable through *in situ*

experiment. Moreover, the amount of data produced and their considerable precision are of primary interest to develop data reduction and learning AI algorithms to go through real time simulation of Smart Manufacturing processes.

We believe that this work helps to follow the increasing computing power of the supercomputers since these available quasi unique supercomputers will be increasingly available in the coming decade. Since the development of supercomputers, each new subsequent generation brings its own set of demonstrations of their capacity to handle more complex problems, higher Reynolds number DNS, etc. This work is part of this logic and is a starting point for further new challenges for continuous flow processes for materials synthesis that include, non isothermal processes, reaction kinetics, and geometry changes (zig-zag channels, T injectors, etc.). Regarding the larger reactors (stirred tank reactor, tower reactor, and fluidized bed reactor), the capability to solve all mixing scales without any turbulence model depends on the operating conditions and the size of the reactor. If DNS is not feasible, Large Eddy Simulation can be used to capture turbulence phenomena in the reactor and yield accurate local and temporal analysis of the flow field and, thereby, resulting in a successful scale up process. It should be noted that LES in large reactors also requires very large simulations.

References

[1] S. Marre, K.F. Jensen, Synthesis of micro and nanostructures in microfluidic systems, Chem. Soc. Rev. 39 (2010) 1183–1202. https://doi.org/10.1039/B821324K.

[2] J. Bałdyga, D. Kubicki, B.Y. Shekunov, K.B. Smith, Mixing effects on particle formation in supercritical fluids, Chemical Engineering Research and Design. 88 (2010) 1131–1141. https://doi.org/10.1016/j.cherd.2010.02.016.

[3] T. Jaouhari, F. Zhang, T. Tassaing, S. Fery-Forgues, C. Aymonier, S. Marre, A. Erriguible, Process intensification for the synthesis of ultra-small organic nanoparticles with supercritical CO2 in a microfluidic system, Chemical Engineering Journal. 397 (2020) 125333. https://doi.org/10.1016/j.cej.2020.125333.

[4] Zhang, Fan, Marre, Samuel, Erriguible, Arnaud, Mixing intensification under turbulent conditions in a high pressure microreactor, Chemical Engineering Journal. 382 (2020) 122859. https://doi.org/10.1016/j.cej.2019.122859.

[5] R.L. Hartman, Flow chemistry remains an opportunity for chemists and chemical engineers, Current Opinion in Chemical Engineering. 29 (2020) 42–50. https://doi.org/10.1016/j.coche.2020.05.002.

[6] M. Berton, J.M. de Souza, I. Abdiaj, D.T. McQuade, D.R. Snead, Scaling continuous API synthesis from milligram to kilogram: extending the enabling benefits of micro to the plant, J Flow Chem. 10 (2020) 73–92. https://doi.org/10.1007/s41981-019-00060-x.

[7] I. Rossetti, M. Compagnoni, Chemical reaction engineering, process design and scale-up issues at the frontier of synthesis: Flow chemistry, Chemical Engineering Journal. 296 (2016) 56–70. https://doi.org/10.1016/j.cej.2016.02.119.

[8] M. Al-Rawashdeh, J. Zalucky, C. Müller, T.A. Nijhuis, V. Hessel, J.C. Schouten, Phenylacetylene Hydrogenation over [Rh(NBD)(PPh3)2]BF4 Catalyst in a Numbered-Up Microchannels Reactor, Ind. Eng. Chem. Res. 52 (2013) 11516–11526. https://doi.org/10.1021/ie4009277.

[9] M. Qiu, L. Zha, Y. Song, L. Xiang, Y. Su, Numbering-up of capillary microreactors for homogeneous processes and its application in free radical polymerization, React. Chem. Eng. 4 (2019) 351–361. https://doi.org/10.1039/C8RE00224J.

[10] J. Zhang, K. Wang, A.R. Teixeira, K.F. Jensen, G. Luo, Design and Scaling Up of Microchemical Systems: A Review, Annual Review of Chemical and Biomolecular Engineering. 8 (2017) 285–305. https://doi.org/10.1146/annurev-chembioeng-060816-101443.

[11] N. Kockmann, M. Gottsponer, D.M. Roberge, Scale-up concept of single-channel microreactors from process development to industrial production, Chemical Engineering Journal. 167 (2011) 718–726. https://doi.org/10.1016/j.cej.2010.08.089.

[12] A. Yamamoto, S. Mori, M. Suzuki, Scale-up or numbering-up of a micro plasma reactor for the carbon dioxide decomposition, Thin Solid Films. 515 (2007) 4296–4300. https://doi.org/10.1016/j.tsf.2006.02.058.

[13] Z. Dong, Z. Wen, F. Zhao, S. Kuhn, T. Noël, Scale-up of Micro- and Milli-Reactors: An Overview of Strategies, Design Principles and Applications, Chemical Engineering Science: X. (2021) 100097. https://doi.org/10.1016/j.cesx.2021.100097.

[14] F. Enzmann, M. Stöckl, A. Zeng, D. Holtmann, Same but different–Scale up and numbering up in electrobiotechnology and photobiotechnology, Eng Life Sci. 19 (2019) 121–132. https://doi.org/10.1002/elsc.201800160.

[15] H. Rehage, M. Bartsch, M. Kind, A new scale-up method for competitive chemical model reactions based on complete similarity, Chemical Engineering Journal. 400 (2020) 125763. https://doi.org/10.1016/j.cej.2020.125763.

[16] J. Bałdyga, R. Czarnocki, B.Y. Shekunov, K.B. Smith, Particle formation in supercritical fluids—Scale-up problem, Chemical Engineering Research and Design. 88 (2010) 331–341. https://doi.org/10.1016/j.cherd.2010.01.019.

[17] F. Zhang, A. Erriguible, S. Marre, Investigating laminar mixing in high pressure microfluidic systems, Chemical Engineering Science. 205 (2019) 25–35. https://doi.org/10.1016/j.ces.2019.03.063.

[18] J. Bałdyga, R. Pohorecki, Turbulent micromixing in chemical reactors — a review, The Chemical Engineering Journal and the Biochemical Engineering Journal. 58 (1995) 183–195. https://doi.org/10.1016/0923-0467(95)02982-6.

[19] J. BALDYGA, J.R. BOURNE, A Fluid Mechanical Approach to Turbulent Mixing and Chemical Reaction Part Ii Micromixing in the Light of Turbulence Theory, Chemical Engineering Communications. 28 (1984) 243–258. https://doi.org/10.1080/00986448408940136.

[20] P. Plouffe, M. Bittel, J. Sieber, D.M. Roberge, A. Macchi, On the scale-up of micro-reactors for liquid–liquid reactions, Chemical Engineering Science. 143 (2016) 216–225. https://doi.org/10.1016/j.ces.2015.12.009.

[21] A.M.D. Jost, S. Glockner, A. Erriguible, Direct numerical simulations of fluids mixing above mixture critical point, The Journal of Supercritical Fluids. 165 (2020) 104939. https://doi.org/10.1016/j.supflu.2020.104939.

[22] D. Sharma, A. Erriguible, G. Gandikota, D. Beysens, S. Amiroudine, Vibration-induced thermal instabilities in supercritical fluids in the absence of gravity, Phys. Rev. Fluids. 4 (2019) 033401. https://doi.org/10.1103/PhysRevFluids.4.033401.

[23] S. Amiroudine, J.-P. Caltagirone, A. Erriguible, A Lagrangian–Eulerian compressible model for the trans-critical path of near-critical fluids, International Journal of Multiphase Flow. 59 (2014) 15–23. https://doi.org/10.1016/j.ijmultiphaseflow.2013.10.008.

[24] Y. Maeta, M. Ota, Y. Sato, R.L. Smith, H. Inomata, Measurements of vapor–liquid equilibrium in both binary carbon dioxide–ethanol and ternary carbon dioxide–ethanol–

water systems with a newly developed flow-type apparatus, Fluid Phase Equilibria. 405 (2015) 96–100. https://doi.org/10.1016/j.fluid.2015.07.025.

[25] https://notus-cfd.org/.

[26] K. Goda, A multistep technique with implicit difference schemes for calculating two- or three-dimensional cavity flows, Journal of Computational Physics. 30 (1979) 76–95. https://doi.org/10.1016/0021-9991(79)90088-3.

[27] A.M.D. Jost, S. Glockner, Direct forcing immersed boundary methods: Improvements to the ghost-cell method, Journal of Computational Physics. 438 (2021) 110371. https://doi.org/10.1016/j.jcp.2021.110371.

[28] M. Coquerelle, S. Glockner, A fourth-order accurate curvature computation in a level set framework for two-phase flows subjected to surface tension forces, Journal of Computational Physics. 305 (2016) 838–876. https://doi.org/10.1016/j.jcp.2015.11.014.

[29] C. Neurohr, A. Erriguible, S. Laugier, P. Subra-Paternault, Challenge of the supercritical antisolvent technique SAS to prepare cocrystal-pure powders of naproxen-nicotinamide, Chemical Engineering Journal. 303 (2016) 238–251. https://doi.org/10.1016/j.cej.2016.05.129.

[30] A.H. Baker, R.D. Falgout, T.V. Kolev, U.M. Yang, Scaling hypre's multigrid solvers to 100,000 cores, Journal Name: High Performance Scientific Computing: Algorithms and Applications, Na, Na, January 24, 2012, Pp. 261-279. (2011). https://digital.library.unt.edu/ark:/67531/metadc864467/ (accessed April 6, 2021).

[31] Q. Liu, J. Logan, Y. Tian, H. Abbasi, N. Podhorszki, J.Y. Choi, S. Klasky, R. Tchoua, J. Lofstead, R. Oldfield, M. Parashar, N. Samatova, K. Schwan, A. Shoshani, M. Wolf, K. Wu, W. Yu, Hello ADIOS: the challenges and lessons of developing leadership class I/O frameworks, Concurrency and Computation: Practice and Experience. 26 (2014) 1453–1473. https://doi.org/10.1002/cpe.3125.

[32] TOP 500 list of the most powerful non-distributed computer systems in the world - https://www.top500.org/lists/top500/list/2020/11/, (2020).

[33] K.R. Sreenivasan, Turbulent mixing: A perspective, PNAS. 116 (2019) 18175–18183. https://doi.org/10.1073/pnas.1800463115.

[34] P.V. Danckwerts, The effect of incomplete mixing on homogeneous reactions, Chemical Engineering Science. 8 (1958) 93–102. https://doi.org/10.1016/0009-2509(58)80040-8.

[35] T. Lemenand, D. Della Valle, C. Habchi, H. Peerhossaini, Micro-mixing measurement by chemical probe in homogeneous and isotropic turbulence, Chemical Engineering Journal. 314 (2017) 453–465. https://doi.org/10.1016/j.cej.2016.12.001.

Acknowledgments

We acknowledge the French National Research Agency for its support (ANR-17-CE07-0029 - SUPERFON). the MCIA (Mésocentre de Calcul Intensif Aquitaine) and GENCI (DARI project number A0062A10815 and “Les Grands Challenges” grant on Joliot-Curie supercomputer) for the HPC resources.